

[OIII] emission line as a tracer of star-forming galaxies at high redshifts: Comparison between H α and [OIII] emitters at $z=2.23$ in HiZELS

T. L. Suzuki,^{1,2*} T. Kodama,^{1,2} D. Sobral,^{3,4} A. A. Khostovan,⁵ M. Hayashi,²
R. Shimakawa,^{1,2} Y. Koyama,⁶ K.-i. Tadaki,⁷ I. Tanaka,⁶ Y. Minowa,^{1,6} M. Yamamoto,^{1,2}
I. Smail,⁸ and P. N. Best⁹

¹Department of Astronomical Science, SOKENDAI (The Graduate University for Advanced Studies), Mitaka, Tokyo 181-8588, Japan

²Optical and infrared Astronomy Division, National Astronomical Observatory of Japan, Mitaka, Tokyo, 181-8588, Japan

³Department of Physics, Lancaster University, Lancaster, LA1, 4YB, UK

⁴Leiden Observatory, Leiden University, PO Box 9513, NL-2300 RA Leiden, the Netherlands

⁵Department of Physics & Astronomy, University of California, 900 University Ave., Riverside, CA 92521, USA

⁶Subaru Telescope, National Astronomical Observatory of Japan, N. A'ohoku Pl., Hilo, HI 96720, USA

⁷Max-Planck-Institut für Extraterrestrische Physik, Giessenbachstrasse, D-85748 Garching, Germany

⁸Centre for Extragalactic Astronomy, Department of Physics, Durham University, South Road, Durham DH1 3LE, UK

⁹SUPA, Institute for Astronomy, Royal Observatory of Edinburgh, Blackford Hill, Edinburgh EH9 3HJ, UK

Accepted 2016 July 07. Received 2016 June 30; in original form 2016 February 11.

ABSTRACT

We investigate the properties of $z=2.23$ H α and [OIII] $\lambda 5007$ emitters using the narrow-band-selected samples obtained from the High- z Emission Line Survey (HiZELS: Sobral et al. 2013). We construct two samples of the H α and [OIII] emitters and compare their integrated physical properties. We find that the distribution of stellar masses, dust extinction, star formation rates (SFRs), and specific SFRs, is not statistically different between the two samples. When we separate the full galaxy sample into three subsamples according to the detections of the H α and/or [OIII] emission lines, most of the sources detected with both H α and [OIII] show $\log(\text{sSFR}_{\text{UV}}) \geq -9.5$. The comparison of the three subsamples suggests that sources with strong [OIII] line emission tend to have the highest star-forming activity out all galaxies that we study. We argue that the [OIII] emission line can be used as a tracer of star-forming galaxies at high redshift, and that it is especially useful to investigate star-forming galaxies at $z > 3$, for which H α emission is no longer observable from the ground.

Key words: galaxies: evolution, galaxies: high-redshift

1 INTRODUCTION

Emission lines from regions ionized by hot, young massive stars are useful as indicators of star formation in distant galaxies. Imaging observations with narrow-band (NB) filters, which can capture redshifted strong emission lines, are a powerful method to construct a star-forming galaxy sample at a particular redshift (e.g. Bunker et al. 1995; Malkan, Teplitz & McLean 1996; Moorwood et al. 2000; Geach et al. 2008; Sobral et al. 2009, 2013; Tadaki et al. 2013; An et al. 2014; Stroe & Sobral 2015). The H α emission line is one of the best tracers of star formation because it is less affected to dust extinction than the ultraviolet (UV) light and the relation between star-formation rates (SFRs) and H α luminosities has been well calibrated in the local Universe (e.g.

Hopkins et al. 2003). This seems to hold at higher redshift. In addition, H α selection has the advantage of recovering the full population of star-forming galaxies (Oteo et al. 2015).

However, the redshift range for H α selection is limited to $z < 2.8$ because H α emission is no longer easily observed beyond $z \sim 2.8$ with ground-based telescopes. Space telescopes, such as the *Spitzer*, have been used for the H α emission line galaxy survey at higher redshift, $z \gtrsim 4.0$, but only using broad band photometry (e.g. Shim et al. 2011; Smit et al. 2015), which is therefore only sensitive to the highest equivalent width lines. In order to investigate star-forming galaxies at $z > 2.8$ with NB imaging observations, it is necessary to use other emission lines at shorter wavelengths than H α , such as [OII] $\lambda 3727$, H β , and [OIII] $\lambda 5007$. With [OII], H β , and [OIII] emission lines, we can reach up to $z \sim 5.2$, 3.7 and 3.6, respectively, from the ground (Khostovan et al. 2015). [OII] and H β are relatively weak lines and so it is more diffi-

* E-mail: suzuki.tomoko@nao.ac.jp

cult to observe them at higher redshift. There is also evidence of higher $[\text{OIII}]/[\text{OII}]$ line ratios at high redshifts, and a potential decline in $[\text{OII}]$ equivalent width (Khostovan et al. 2016). On the other hand, strong $[\text{OIII}]$ detections that are comparable to $\text{H}\alpha$ from high-redshift star-forming galaxies have been reported by recent near-infrared (NIR) spectroscopic observations (e.g. Holden et al. 2014; Masters et al. 2014; Steidel et al. 2014; Shimakawa et al. 2015; Shapley et al. 2015). Such strong $[\text{OIII}]$ emission indicates extreme interstellar medium (ISM) conditions in high-redshift galaxies, and this is likely to be due to their lower metallicities and/or higher ionization parameters (e.g. Nakajima & Ouchi 2014). Also, $[\text{OIII}]$ emission in the rest-frame optical is less sensitive to dust extinction than the UV light. In these respects, it is expected that the $[\text{OIII}]$ emission line can be used to select star-forming galaxies at $z\sim 3\text{--}3.6$, corresponding to $\sim 1\text{--}1.5$ billion years before the peak epoch of galaxy formation and evolution at $z\sim 2$ (e.g. Hopkins & Beacom 2006; Khostovan et al. 2015). Some studies have been constructing $[\text{OIII}]$ (+ $\text{H}\beta$) emitter samples at $z>3$, and have investigated their star-forming activity or the evolution of the luminosity function (Teplitz, Malkan & McLean 1999; Maschietto et al. 2008; Labbé et al. 2013; Smit et al. 2014; Suzuki et al. 2015; Khostovan et al. 2015, 2016). Star-forming activity and other physical properties of galaxies at $z>3$ have also been investigated with UV-selected galaxies, such as Lyman Break Galaxies (e.g. Stark et al. 2009; González et al. 2010; Reddy et al. 2012; Stark et al. 2013; Tasca et al. 2015). By using $[\text{OIII}]$ emission as a tracer at $z>3$, it is expected that we can obtain further understanding about galaxy formation and evolution before the peak epoch of galaxy assembly.

However, there are possible biases resulting from the use of $[\text{OIII}]$ emission as a star-forming indicator. For example, the $[\text{OIII}]$ emission line originates from ionized regions not only caused by hot, young massive stars in star-forming regions but also by active galactic nuclei (AGNs; e.g. Zakamska et al. 2004). Due to the shorter wavelength of $[\text{OIII}]$ (5007\AA) with respect to $\text{H}\alpha$ (6563\AA), samples of $[\text{OIII}]$ -selected galaxies may be inherently biased against dusty systems in comparison to an $\text{H}\alpha$ -selected sample. As already mentioned above, galaxies with strong $[\text{OIII}]$ emission might be biased towards galaxies with lower metallicities and/or higher ionization states, resulting in a potential bias towards galaxies with lower stellar masses given the well-known mass–metallicity relation of star-forming galaxies (e.g. Tremonti et al. 2004; Erb et al. 2006a; Stott et al. 2014; Troncoso et al. 2014).

At $z\sim 0$ and $z\sim 1.5$, the selection biases between $\text{H}\alpha$ and $[\text{OIII}]$ have been investigated using the SDSS galaxies and FMOS-COSMOS galaxies (Silverman et al. 2015) by Juneau et al. (in preparation, private communication). Their samples are selected based on $\text{H}\alpha$ and $[\text{OIII}]$ luminosities. Mehta et al. (2015) investigated the relation between $\text{H}\alpha$ and $[\text{OIII}]$ luminosities for galaxies at $z\sim 1.5$ in the *HST*/WFC3 Infrared Spectroscopic Parallel Survey (WISP; Atek et al. 2010), and derived the $\text{H}\alpha$ – $[\text{OIII}]$ bivariate luminosity function at $z\sim 1.5$. Sobral et al. (2012) and Hayashi et al. (2013) investigated the relation between the NB-selected $\text{H}\alpha$ and $[\text{OII}]$ emission line galaxies at $z\sim 1.47$. They discussed the lack of redshift evolution of the $[\text{OII}]/\text{H}\alpha$ ratio from $z\sim 0$ to 1.5 (Sobral et al. 2012), and also found that the $[\text{OII}]$ -selected galaxies tend to be biased towards less dusty galaxies with respect to the $\text{H}\alpha$ -selected galaxies (Hayashi et al. 2013). At $z>2$, some studies have already performed the comparisons between the samples of star-forming galaxies selected by different optical emission lines, such as $\text{H}\alpha$ and $\text{Ly}\alpha$, or by other selection methods (e.g. Oteo et al. 2015; Hagen et al. 2016; Matthee et al. 2016;

Shimakawa et al. 2016). However, the comparison of the physical quantities between $\text{H}\alpha$ and $[\text{OIII}]$ -selected galaxy samples has not been done yet at $z>2$. Such a comparison is necessary in order to accurately interpret results from $[\text{OIII}]$ surveys at $z>3$.

In this study, we use the NB-selected $[\text{OIII}]$ and $\text{H}\alpha$ emission line galaxies at $z=2.23$, obtained by HiZELS (the High- z Emission Line Survey; Best et al. 2013; Sobral et al. 2009, 2012, 2013, 2014), a large NB imaging survey. The $[\text{OIII}]$ and $\text{H}\alpha$ emission lines are observed using the NB_H and NB_K filters, respectively. This combination of NB filters allows for the creation of a suitable sample to investigate possible selection biases between the $[\text{OIII}]$ and $\text{H}\alpha$ emission line galaxies at high redshift. We compare the integrated quantities, such as stellar masses, dust extinction, and star formation rates (SFRs), and investigate whether there are any systematic differences between these physical quantities. Some galaxies are detected with both the $[\text{OIII}]$ and $\text{H}\alpha$ emission lines. We investigate the physical properties of the galaxies depending on the detectability of their $[\text{OIII}]$ and $\text{H}\alpha$ emission lines.

This paper is organized as follows: In §2, we briefly introduce the NB imaging survey, HiZELS, and describe how the $[\text{OIII}]$ and $\text{H}\alpha$ emission line galaxies at $z\sim 2$ are selected. We also present the method for deriving the integrated physical quantities. Then, we show our results in §3. We present the relationship between stellar masses and SFRs for the two emitter samples, and compare the number distribution of the global physical quantities between the $\text{H}\alpha$ and $[\text{OIII}]$ emitters. Moreover, we divide our full sample into three subsamples according to the detections of the $\text{H}\alpha$ and/or $[\text{OIII}]$ emission lines, and compare the distributions of physical quantities among the three subsamples. We summarize this study in §4. We assume the cosmological parameters of $\Omega_m = 0.3$, $\Omega_\Lambda = 0.7$, and $H_0 = 70$ [$\text{km s}^{-1}\text{Mpc}^{-1}$]. Throughout this paper all the magnitudes are given in AB magnitude system (Oke & Gunn 1983), and the Salpeter initial mass function (IMF; Salpeter 1955) is adopted for the estimation of the stellar masses and SFRs¹.

2 DATA AND ANALYSIS

2.1 NB imaging survey in the COSMOS field

HiZELS is a systematic NB imaging survey using NB filters in the J , H , and K -bands of the Wide Field CAMERA (WFCAM; Casali et al. 2007) on the United Kingdom Infrared Telescope (UKIRT), and the NB921 filter of the Suprime-Cam (Miyazaki et al. 2002) on the Subaru Telescope (Sobral et al. 2012, 2013). Emission line galaxy samples used in this study are based on the HiZELS catalogue in the Cosmological Evolution Survey (COSMOS; Scoville et al. 2007) field.

An advantage in the design of the NB filters is the symmetry in respect to their wavelength centers, such that an $[\text{OIII}]$ emission can be detected in NB_H and $\text{H}\alpha$ in $\text{NB}_K(\text{H}_2\text{S1})$ with both detections occurring at $z=2.23$ (Table 1 and Figure 1). Matthee et al. (2016) has recently presented NB392 observations with the Isaac Newton Telescope which target $\text{Ly}\alpha$ at $z=2.23$ in a similar way, and investigated the $\text{Ly}\alpha$ properties of the $z=2.23$ $\text{H}\alpha$ emitters.

¹ Stellar mass estimated assuming the Salpeter IMF can be scaled to those assuming the Chabrier (Chabrier 2003) and Kroupa (Kroupa 2002) IMF by dividing by a factor of ~ 1.7 and 1.6, respectively (Pozzetti et al. 2007; Marchesini et al. 2009).

Table 1. NB filters in the H and K -band used in HiZELS (Sobral et al. 2013).

Filter	λ_c [μm]	FWHM [\AA]	Redshift coverage
NB _H	1.617	211	2.23 ± 0.021 for $[OIII]\lambda 5007$
NB _K	2.121	210	2.23 ± 0.016 for $H\alpha$

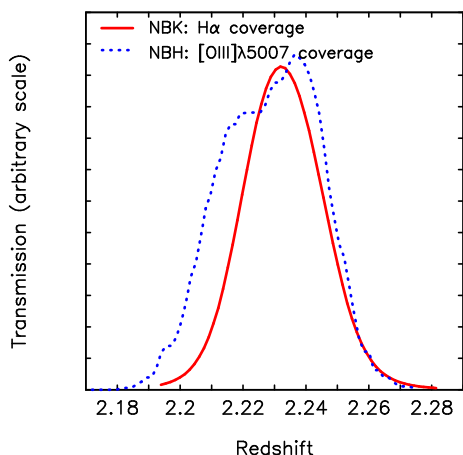


Figure 1. A comparison between the NB_H redshift coverage for the $[OIII]\lambda 5007$ emission line (dotted line) and the NB_K redshift coverage for the $H\alpha$ emission line (solid line). The redshift coverage of $[OIII]\lambda 5007$ is slightly wider than that of $H\alpha$ as mentioned in §2.2.3.

2.2 Selection of $[OIII]$ and $H\alpha$ emitters

The catalogs of $H\alpha$ emitters and $[OIII]$ emitters at $z=2.23$ used in this study are taken from Sobral et al. (2013) and Khostovan et al. (2015), respectively. The selection criteria of these emitters are described in detail in the two papers. Here we briefly summarize the selection methods in the following subsections.

2.2.1 Selection of NB excess sources

The sources that are significantly brighter in the NB than in the broad-band (BB) are selected as NB emitters using BB-NB color versus NB magnitude diagrams (Figure 3 in Sobral et al. 2013). A parameter Σ is introduced to quantify the significance of a NB excess relative to 1σ photometric error (Bunker et al. 1995). This parameter Σ is represented as a function of NB magnitude as follows (Sobral et al. 2013):

$$\Sigma = \frac{1 - 10^{-0.4(BB-NB)}}{10^{-0.4(ZP-NB)} \sqrt{\pi r_{\text{ap}}^2 (\sigma_{\text{NB}}^2 + \sigma_{\text{BB}}^2)}}, \quad (1)$$

where NB and BB are NB and BB magnitudes, ZP is the zero-point of the NB (the BB images are scaled to have the same ZP as the NB images), r_{ap} is the aperture radius in pixel, and σ_{NB} and σ_{BB} are the rms per pixel of the NB and BB images, respectively (Sobral et al. 2013). The criterion is set to be $\Sigma > 3$ to sample secure NB emitters. A rest-frame equivalent width (EW) limit of $\text{EW}_{\text{rest}} = 25\text{\AA}$ is also applied (Sobral et al. 2013; Khostovan et al. 2015). These selection criteria are applied for both NB_H and NB_K.

2.2.2 Redshift identification

The redshift identification of the NB emitters for NB_H and NB_K is performed based on the photometric redshifts, broad-band colors (color-color selections) and the spectroscopic redshifts. Here we give the priorities in the following order (from higher to lower): (1) spectroscopic redshifts, (2) photometric redshifts, and (3) color-color selections (Sobral et al. 2013; Khostovan et al. 2015). If the sources are spectroscopically confirmed to be the targeted line emitters, they are firmly identified as the $H\alpha$ or $[OIII]$ emitters. The numbers of such $H\alpha$ and $[OIII]$ emitters which are confirmed with the spectroscopic redshifts are however only three and one, respectively (Sobral et al. 2013; Khostovan et al. 2015). Secondly, if the sources have the photometric redshifts within $1.7 < z_{\text{phot}} < 2.8$, they are robustly identified as the $H\alpha$ or $[OIII]$ emitters at $z \sim 2.23$. Here, the photometric redshifts are taken from the catalog of Ilbert et al. (2009).

Color-color diagrams are also applied for the redshift separation of the emitters. For the NB_K emitters, the $(z-K)$ versus $(B-z)$ color-color diagram is used to sample additional faint $H\alpha$ emitters at $z \sim 2$, which lack reliable photometric redshifts. In addition to the BzK selection, the photometric redshift criteria of $z_{\text{photo}} < 3.0$ or the color-color diagram of $(B-R)$ versus $(U-B)$ are applied to remove higher-redshift sources (Sobral et al. 2013). For the NB_H emitters, the BzK color-color diagram is used to remove the foreground at $z < 1.5$, and additionally, the $(z-K)$ vs $(i-z)$ diagram is applied to separate the potential $z=1.47$ $H\alpha$ emitters. In order to remove the higher redshift sources, the $(V-z)$ versus $(U-V)$ diagram is used (Khostovan et al. 2015).

Note that Sobral et al. (2013) and Khostovan et al. (2015) applied slightly different color-color diagrams because the other strong emission lines that could contaminate the samples (and hence the redshifts of the foreground and background galaxies that need to be excluded) are different for the two NB filters. We confirm that there is no systematic difference in the distributions of the $H\alpha$ and $[OIII]$ emitters at $z \sim 2.23$ on any of the color-color diagrams mentioned above. We consider that the color-color selection for the NB_K and NB_H emitters are consistent with each other. In this study, we follow the color-color selection criteria for each NB filter. This difference does not cause any systematic differences between the two emitter samples.

The number of the redshift-identified $H\alpha$ and $[OIII]$ emitters at $z=2.23$ is 513 and 172, respectively.

2.2.3 AGN contribution of the two emitter samples

We use the X-ray observations and *Spitzer*/IRAC colors to investigate the contribution of AGNs to our $H\alpha$ and $[OIII]$ emitter samples at $z=2.23$.

The redshift-identified $H\alpha$ and $[OIII]$ emitters are matched with the X-ray point source catalog from the *Chandra* COSMOS Legacy survey (Civano et al. 2016) in order to identify obvious AGNs. The fraction of the X-ray-detected sources is only 2.3% and 3.5% for the $H\alpha$ and $[OIII]$ emitters, respectively. We remove these X-ray-detected sources from the two emitter samples.

We also estimate the fractions of obscured AGN candidates in the $H\alpha$ and $[OIII]$ emitters. The colors in *Spitzer*/IRAC four channels are commonly used to identify obscured AGNs (e.g. Lacy et al. 2007; Stern et al. 2005; Donley et al. 2008). We here use only the sources detected at more than the 2σ level in all four channels of IRAC, which limited our $H\alpha$ and $[OIII]$ emitter samples to only 15% and 17% (76 and 29 sources), respectively. When we

use the $S_{5.8}/S_{3.6}-S_{8.0}/S_{4.5}$ diagram with the selection criteria of Donley et al. (2012), the fraction of the emitters which can be classified as AGNs is $\sim 14\%$ for both the $H\alpha$ and [OIII] emitter samples. This fraction must be an over estimation of the true fraction. Given the fact that the bright $H\alpha$ emitters are more likely to be AGNs (Sobral et al. 2016), using only the emitters that are bright enough in all four IRAC channels might cause a higher AGN fraction than the true fraction.

We note that the fractions of the X-ray-detected sources or IRAC-color-selected AGNs are not different between the $H\alpha$ emitters and [OIII] emitters at $z=2.23$, indicating that the [OIII] emitters do not necessarily show the higher fraction of AGNs as compared to the $H\alpha$ emitters.

2.2.4 Final samples of [OIII] and $H\alpha$ emitters at $z=2.23$

The HiZELS NB survey in the COSMOS field covers a very wide area of 1.6 deg^2 , but the survey depth is different among the WFCAM pointings and among different NB filters (see Sobral et al. 2013). In this study, in order to ensure the same flux limit for both NB-selected samples, we use the sources in the deepest pointings only. The minimum exposure times are 107 ks and 62.5 ks for NB_H and NB_K , respectively. The survey area is then limited to the central $\sim 0.2 \text{ deg}^2$. The 3σ limiting fluxes for NB_H and NB_K are $3.60 \times 10^{-17} \text{ erg s}^{-1} \text{ cm}^{-2}$ and $2.96 \times 10^{-17} \text{ erg s}^{-1} \text{ cm}^{-2}$, respectively. In this study, we apply the same flux limit of $3.6 \times 10^{-17} \text{ erg s}^{-1} \text{ cm}^{-2}$ ([OIII] flux for NB_H and $H\alpha$ + [NII] flux for NB_K). As a result, 49 [OIII] emitters and 44 $H\alpha$ emitters remain in our final samples.

In §3.4, we focus on the galaxies detected with both [OIII] and $H\alpha$ emission lines (hereafter, dual emitters). When we search for the counterpart line, we lower the line detection threshold, as we can trust more the existence of a line at the expected wavelength in the other NB filter. We thus use the lower NB_H (NB_K) excess criteria, namely, $EW \geq 15 \text{ \AA}$ and/or $\Sigma \geq 2$. We find 23 dual emitters in total. Among them, ten sources satisfy the original NB excess criteria of both NB_H and NB_K , indicating that they have the strong [OIII] and $H\alpha$ emission lines. Eleven (two) sources are the $H\alpha$ ([OIII]) emitters with the relatively weak [OIII] ($H\alpha$) emission lines. The number of sources in each sample used in this study is summarized in Table 2.

We note that the transmission curves of NB_H and NB_K filters are not completely matched (Figure 1). The wavelength coverage of the two filters are transformed to the redshift space for each line in Figure 1 and Table 1. It turns out that $\sim 10\%$ of the NB_H redshift coverage ([OIII] $\lambda 5007$) is completely out of the NB_K redshift coverage ($H\alpha$). In terms of FWHM ranges of the two NB filters, however, 24% of the NB_H coverage is out of the NB_K coverage in redshift space. This mismatch of the redshift coverage is not critical when we compare the $H\alpha$ and [OIII] emitters in §3.3. However, when we consider the sample of galaxies detected only by the [OIII] emission line, the impact of this difference could be larger. The redshift mismatch might cause the loss of $H\alpha$ flux from the galaxies which actually have the strong enough $H\alpha$ emission line, and thus the observed [OIII]/ $H\alpha$ ratio would become different from the intrinsic ratio. In such a case, the $H\alpha$ flux would seem much lower with respect to [OIII], and in the extreme case, the emitter would appear as an [OIII] emitter with no $H\alpha$ emitter counterpart. Therefore, “[OIII]-single-emitters” (see Table 2 for the definition) may include some dual emitters, and one should use caution when comparing the properties of this subsample with others.

2.3 Contribution of $H\beta$ and [OIII] $\lambda 4959$ emitters

There are the two lines which are close to our target line ([OIII] $\lambda 5007$), namely, [OIII] $\lambda 4959$ and $H\beta$ at $\lambda=4861 \text{ \AA}$. The wavelength coverage of NB_H is too narrow to include both the $H\beta$ and [OIII] lines simultaneously. On the other hand, the [OIII] doublet lines can be detected at the same time at the opposite edges of NB_H for some galaxies in a narrow redshift range of $\Delta z \sim 0.01$. However, the fraction of such emitters is expected to be small ($\sim 7\%$ of the [OIII]+ $H\beta$ emitters at $z=1.47$; see the full analysis from spectroscopy in Sobral et al. 2015).

However, as is also noted in Khostovan et al. (2015), $H\beta$ or [OIII] $\lambda 4959$ at slightly different redshifts can not be actually distinguished from our target [OIII] $\lambda 5007$ emitters at $z=2.23$ by photometric redshifts and broad-band color selections because their redshifts are too close to separate only with photometric data. We estimate the fraction of such $H\beta$ and [OIII] $\lambda 4959$ emitters included in the NB_H emitters by considering the luminosity functions of $H\beta$ and [OIII] $\lambda 4959$.

The luminosity functions of the $H\beta$ and [OIII] $\lambda 4959$ line are determined by converting the luminosity functions of the $H\alpha$ (Sobral et al. 2013) and [OIII] line (Colbert et al. 2013) assuming the line ratios of $H\alpha/H\beta \sim 5$ incorporating the effects of dust based on the observations of Hayashi et al. (2011) and Shimakawa et al. (2015), and [OIII] $\lambda 5007$ /[OIII] $\lambda 4959 = 3$ (the theoretical ratio; Storey & Zeppen 2000), respectively. With our 3σ detection limit of $3.60 \times 10^{-17} \text{ erg s}^{-1} \text{ cm}^{-2}$, the contribution of the $H\beta$ emitters is estimated to be $\sim 3\%$. Similarly, the contribution of the [OIII] $\lambda 4959$ emitters is estimated to be 25%. Sobral et al. (2015) performed the spectroscopic follow-up observations for the [OIII] + $H\beta$ emitters at $z \sim 1.47$ obtained by HiZELS. They found that the [OIII] $\lambda 5007$ emitters are dominant population, constituting $\sim 50\%$ of the full sample of the [OIII] + $H\beta$ emitters. The [OIII] $\lambda 4959$ and $H\beta$ emitters represent 27% and 16% of the sample, respectively. The remaining 7% of sources are detected with both of the [OIII] doublet lines at the opposite edges of the NB filter. The fraction of [OIII] $\lambda 4959$ emitters is consistent with our estimation using the luminosity functions, although the fraction of the $H\beta$ emitters of our estimation is smaller than that of Sobral et al. (2015). This is probably due to the difference of the targeted redshifts ($z=1.47$ versus 2.23). Considering that the [OIII] emission line becomes more prominent at higher redshifts (e.g. Faisst et al. 2016), and that the fraction of the $H\beta$ emitters among the [OIII]+ $H\beta$ emitters decreases with luminosity (Sobral et al. 2015), the fraction of the $H\beta$ emitters might decrease at higher redshifts.

We note that the fraction of [OIII] $\lambda 4959$ is not negligible. However, the galaxies with strong [OIII] $\lambda 4959$ should have even stronger [OIII] $\lambda 5007$ emission given the line ratio. Therefore, the [OIII] $\lambda 4959$ emitters and the emitters which are detected with both the [OIII] doublet lines can also be regarded as the [OIII] $\lambda 5007$ emitters, although they are still missed out from the dual emitter sample. Spectroscopic follow-up observations are necessary to accurately quantify the contribution of the $H\beta$ and [OIII] $\lambda 4959$ emitters at $z \sim 2$.

We note that the grism spectroscopy of *HST* also suffers from blending of the $H\beta$, [OIII] 4959 and 5007 emission lines. The wavelength resolution of *HST*/WFC3 grism is not enough to resolve the [OIII] doublet lines. In the WISP survey, for example, they tried to deblend the [OIII] 4959 and 5007 lines by using a multi-Gaussian model with the fixed [OIII] $\lambda 5007$ /[OIII] $\lambda 4959$ ratio (Atek et al. 2010, 2014).

In summary, taking into account the relative strength of [OIII] $\lambda 5007$ as compared to [OIII] $\lambda 4959$ and $H\beta$, we consider that

Table 2. Summary of samples and subsamples used in this study.

Name	Number of sources	Notes
$H\alpha$ emitters	44	–
[OIII] emitters	49	–
$H\alpha$ -single-emitters	23	$H\alpha$ emitters with no [OIII] emitter counterpart
[OIII]-single-emitters	37 ⁱ⁾	[OIII] emitters with no $H\alpha$ emitter counterpart
Dual emitters	23	$H\alpha$ + [OIII] emitters (dual emitters)

i) We note that the number of the [OIII] emitters with no $H\alpha$ emitter counterpart is larger than that of the $H\alpha$ emitters with no [OIII] emitter counterpart. Some [OIII] emitters might be [OIII] λ 4959 or $H\beta$ emitters as discussed in §2.3, and thus they do not have $H\alpha$ emitter counterparts.

the majority of the NB_H emitters are the [OIII] λ 5007 emitters once we apply the redshift identification in §2.2.2. Moreover, our [OIII] λ 5007 line flux is not contaminated by [OIII] λ 4959 or $H\beta$ at the same redshift for most of the emitters.

2.4 Estimation of physical quantities

2.4.1 Stellar masses

Stellar masses are estimated from spectral energy distribution (SED) fitting with a stellar population synthesis model based on the public code EAZY (Brammer, van Dokkum & Coppi 2008) and FAST (Kriek et al. 2009). We use 16 photometric band data, FUV , NUV , u , B , V , g , r , i , I_c , z , J , K , 3.6, 4.5, 5.8, and 8.0 μm obtained from the photometric catalog of Ilbert et al. (2009). For the sources detected with NB_K , $H\alpha$ + [NII] line fluxes are subtracted from the K -band fluxes before performing the SED fitting. The contribution of $H\alpha$ + [NII] fluxes corresponds to $\sim 20\%$ of the K -band fluxes on average. The redshift of the galaxies is fixed to $z=2.23$. We use the stellar population synthesis model of Bruzual & Charlot (2003) with the Salpeter IMF (Salpeter 1955) and the dust extinction law of Calzetti et al. (2000). We assume exponentially declining star formation history (SFH) in the form of $\text{SFR} \sim \exp(-t/\tau)$, with $\log(\tau/\text{yr})=8.5\text{--}10.0$ in steps of 0.1, and the metallicities of 0.004, 0.008, 0.02 (solar) and 0.05, similar to the analysis of Sobral et al. (2014).

2.4.2 Star formation rates and dust extinctions

We estimate the rest-frame 1600 \AA luminosity at $z=2.23$ using the V -band photometry from Ilbert et al. (2009), and convert $L(1600\text{\AA})$ to the UV star formation rates (SFRs) as mentioned below. Dust extinction is corrected for using the slope of the rest-frame UV continuum spectrum (e.g. Meurer, Heckman & Calzetti 1999; Heinis et al. 2013). The UV slope β is defined as $f_\lambda \propto \lambda^\beta$. We estimate β by fitting a linear function to the five broad-band photometries from the B to i -bands. The slope β is converted to the dust extinction A_{FUV} with the following equation from Heinis et al. (2013):

$$A_{FUV} = 3.4 + 1.6\beta. \quad (2)$$

Then, the intrinsic flux density $f_{v,\text{int}}$ is obtained from

$$f_{v,\text{int}} = f_{v,\text{obs}} 10^{0.4A_{FUV}}, \quad (3)$$

and SFRs are estimated from UV luminosities adopting the equation from Madau, Pozzetti & Dickinson (1998):

$$\begin{aligned} \text{SFR} (M_\odot \text{yr}^{-1}) &= \frac{4\pi D_L^2 f_{v,\text{int}}}{(1+z) \times 8 \times 10^{27} (\text{erg s}^{-1} \text{cm}^{-2} \text{Hz}^{-1})} \\ &= \frac{L(1600\text{\AA})}{8 \times 10^{27} (\text{erg s}^{-1} \text{Hz}^{-1})}, \end{aligned} \quad (4)$$

where D_L is the luminosity distance.

For the sources with $H\alpha$ detections, we also derive $\text{SFR}_{H\alpha}$. Since we only obtain $H\alpha$ + [NII] fluxes from the NB_K imaging observations, [NII] line fluxes should be removed from the total NB fluxes. The [NII] fluxes are removed using the correlation of the two line ratio with the EW of $H\alpha$ + [NII] as shown in Sobral et al. (2013). We then estimate $\text{SFR}_{H\alpha}$ using the relation between SFRs and $H\alpha$ luminosities of Kennicutt (1998):

$$\text{SFR}_{H\alpha} (M_\odot \text{yr}^{-1}) = 7.9 \times 10^{-42} \frac{L_{H\alpha}}{\text{ergs}^{-1}}. \quad (5)$$

The dust extinction for $H\alpha$ emission is estimated from A_{FUV} by assuming the Calzetti extinction law (Calzetti et al. 2000). We assume that there is no extra extinction for the nebular emissions compared to the stellar extinction, i.e. $E(B-V)_{\text{stellar}} = E(B-V)_{\text{nebula}}$ (e.g. Erb et al. 2006b; Reddy et al. 2010, 2015) although this is still under the debate. We compare the SFRs derived from two different indicators, UV luminosities and $H\alpha$ luminosities, in Figure 2. We find that the SFR_{UV} and $\text{SFR}_{H\alpha}$ are broadly consistent with each other within a factor of 2, indicating that we can estimate SFRs reasonably well with UV luminosities with dust correction based on the UV slope. For the three sources with the highest SFR_{UV} , their SFRs derived from $H\alpha$ are apparently smaller than those from UV luminosities. The difference between the dust extinction to the ionized gas and stellar continuum might be involved in such an inconsistency, because previous studies targeting the galaxies with relatively higher SFRs or higher stellar masses on average have indicated that the ionized gas are more strongly affected by dust extinction than the stellar continuum (e.g. Förster Schreiber et al. 2009; Kashino et al. 2013). In the following analysis, SFRs of all the sources are represented by SFR_{UV} . This allows us to compare SFRs between the $H\alpha$ emitters and [OIII] emitters with the same SFR indicator.

3 RESULTS AND DISCUSSION

3.1 [OIII]/ $H\alpha$ flux ratios

We firstly investigate the [OIII]/ $H\alpha$ ratios of the samples used in this study. In Figure 3, we compare the dust-extinction-corrected

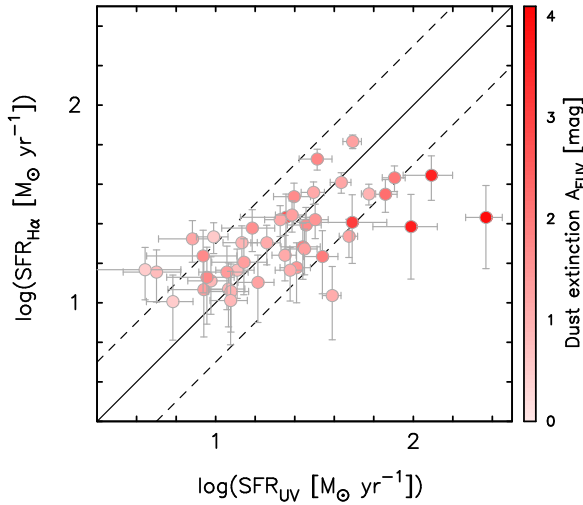


Figure 2. Comparison of SFRs derived from UV luminosities and $H\alpha$ luminosities for the $H\alpha$ emitters at $z=2.23$. Dust extinction correction is based on the UV slope β . We assume that there is no extra extinction to emission lines as compared to the extinction to the stellar continuum. The strength of colors are corresponding to the dust extinction A_{FUV} . The solid line represents the case where the two SFRs are identical, and the dashed lines represents the case where a difference between the two is a factor of 2.

$H\alpha$ and $[OIII]$ fluxes of the three subsamples (Table 2), and examine their $[OIII]/H\alpha$ ratios. For the $H\alpha$ -single-emitters and $[OIII]$ -single-emitters, their $[OIII]$ or $H\alpha$ fluxes are shown as the upper limit values. We note that there is an uncertainty of the $[OIII]/H\alpha$ ratios due to the slightly different wavelength coverage between NB_H and NB_K (§2.2.4).

Steidel et al. (2014) and Shapley et al. (2015) investigated the $[OIII]/H\beta$ ratios of star-forming galaxies at $z\sim 2$. Converting their $[OIII]/H\beta$ ratios to $[OIII]/H\alpha$ ratios by assuming the intrinsic $H\alpha/H\beta$ ratio of 2.86 (case B), the intrinsic $[OIII]/H\alpha$ ratios ($\log([OIII]/H\alpha)$) are estimated to be $\sim -0.45 - 0.4$ for the samples of Steidel et al. (2014) and $\sim -0.45 - 0.19$ of Shapley et al. (2015). In Faisst et al. (2016), the intrinsic $[OIII]/H\alpha$ ratios of star-forming galaxies at $z\sim 2.2$ are estimated to be roughly $-0.4 - 0.2$. Figure 3 shows that our samples have $\log([OIII]/H\alpha) \sim -0.6 - 0.6$, and therefore, although there are still uncertainties regarding the $[OIII]/H\alpha$ ratios shown in Figure 3, our samples of the NB-selected galaxies at $z=2.23$ seem to have broadly consistent $[OIII]/H\alpha$ ratios with respect to other galaxy samples at the same epoch selected with different methods.

3.2 Stellar mass – SFR relation

We investigate the relation between stellar masses and UV-derived SFRs (SFR_{UV}) for the NB-selected galaxies at $z=2.23$ (Figure 4). It is well known that there is an apparent correlation between the stellar mass and SFR of moderately star-forming galaxies, called the “star-forming main sequence” (e.g. Daddi et al. 2007; Elbaz et al. 2007; Noeske et al. 2007; Koyama et al. 2013; Kashino et al. 2013; Whitaker et al. 2014).

In Figure 4, we plot such a diagram using SFR_{UV} and see a positive correlation for both of our $H\alpha$ emitters and $[OIII]$ emitters. Importantly, the distributions of the two samples on the stellar mass–SFR diagram are not significantly different from each other. The dual emitters are also shown in the plot, and we discuss this

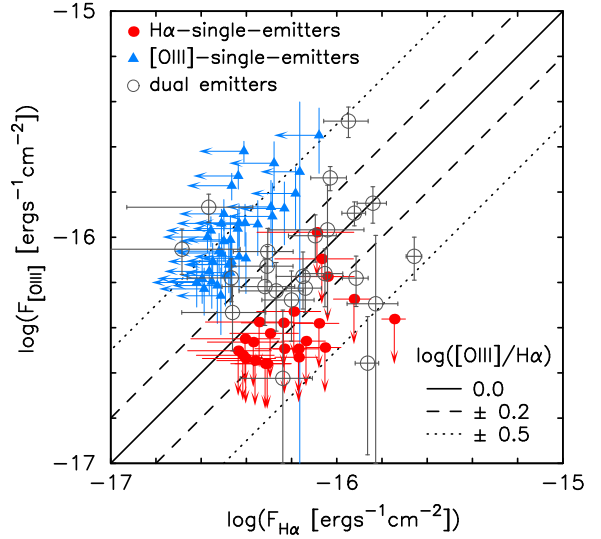


Figure 3. The relation between $H\alpha$ and $[OIII]\lambda 5007$ flux for the three subsamples. Flux of each emission is corrected for dust extinction based on A_{FUV} by assuming the extinction curve of Calzetti et al. (2000) and $E(B - V)_{\text{stellar}} = E(B - V)_{\text{nebula}}$ as mentioned in §2.4.2. Filled circles, filled triangles, and open circles represent the $H\alpha$ -single-emitters, $[OIII]$ -single-emitters, and dual emitters, respectively. For the $H\alpha$ -single-emitters and $[OIII]$ -single-emitters, their $[OIII]$ or $H\alpha$ fluxes are shown as the upper limit values using the 2σ limiting flux. The solid, dashed, and dotted line corresponds to $\log([OIII]/H\alpha) = 0.0, \pm 0.2$, and ± 0.5 , respectively.

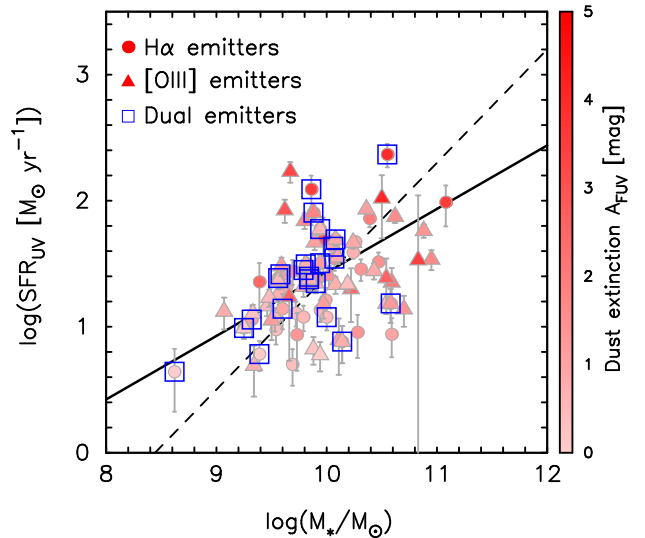


Figure 4. Stellar mass and SFR relation for the NB-selected galaxies at $z=2.23$. SFRs are derived from UV luminosities and corrected for dust extinction using the UV slope β . Circles and triangles represent $H\alpha$ emitters and $[OIII]$ emitters, respectively. The strength of the colors corresponds to A_{FUV} . The dual emitters, as defined in §2.2.4, are shown as blue open squares. The dashed line shows the stellar mass– SFR_{UV} relation for the UV-selected galaxies at $z\sim 2$ from Daddi et al. (2007). The solid line represents the relation derived from the $H\alpha$ emitters at $z=2.2$ with $M_* \geq 10^{10} M_\odot$ from HiZELS (Koyama et al. 2013), although SFRs are based on $H\alpha$ luminosities rather than UV luminosities.

population in §3.4. Each symbol is color-coded according to the dust extinction A_{FUV} . We can see the trend that the galaxies with higher stellar mass and/or higher SFR typically show higher dust extinction.

3.3 Comparison of physical quantities between the $H\alpha$ and [OIII] emitters

In this section, we compare the two samples, the $H\alpha$ and [OIII] emitters at $z=2.23$, regardless of whether they are the dual emitters or not. We compare the distribution of the integrated physical quantities, such as a stellar mass, dust extinction, SFR_{UV} , and specific SFR_{UV} ($sSFR = SFR/M_*$ [yr^{-1}]), in Figure 5.

In order to investigate whether there are any systematic differences between the two samples, we use a Kolmogorov-Smirnov (KS) test. The p -values from the KS-test are summarized in Table 3. The p -values for all the physical quantities are larger than 0.05, meaning that the $H\alpha$ emitters and [OIII] emitters are consistent with being drawn from the same population. As shown in Figure 5, the galaxies selected by [OIII] emission at $z=2.23$ occupy almost the same ranges in their integrated properties with those of the galaxies selected by $H\alpha$. This suggests that the [OIII]-selected galaxies trace the same general population as the $H\alpha$ -selected galaxies.

3.4 $H\alpha$ + [OIII] emitters at $z \sim 2.23$

3.4.1 Comparison of the three subsamples

We divide the whole emitter sample into three subsamples according to the detections of the $H\alpha$ and [OIII] emission lines as defined in §2.2.4, namely, the galaxies detected with only the $H\alpha$ emission line ($H\alpha$ -single-emitters), the galaxies detected with only the [OIII] emission line ([OIII]-single-emitters), and the ‘‘dual emitters’’ which are detected with both the $H\alpha$ and [OIII] lines. The numbers of galaxies in each sample are summarized in Table 2.

Figure 6 shows the number distribution of the same physical quantities as in Figure 5 but now for the three subsamples. We perform a KS-test, and the resulting p -values are listed in Table 3. For almost all of them, except for only two particular cases, the p -values are greater than 0.05, and we can statistically consider that all the emitter samples are drawn from intrinsically similar distributions.

3.4.2 Two exceptions: High $sSFR_{UV}$ of the dual emitters

The two exceptions are the comparison of $sSFR_{UV}$ between the $H\alpha$ -single-emitters and the dual emitters, and between the [OIII]-single-emitters and the dual emitters. Figure 6 shows that the dual emitters tend to have slightly higher $sSFR_{UV}$ as compared to the other two subsamples.

Considering the comparison between the $H\alpha$ -single-emitters and the dual emitters, this result indicates that the star-forming galaxies with relatively stronger [OIII] emission lines tend to have higher star formation activity with respect to their stellar masses. This can be understood by the following arguments. Since high $sSFR_{UV}$ produces more UV flux per volume, it leads to more extreme ISM condition characterized by the higher ionization parameter and thus showing the strong [OIII] emission line with respect to $H\alpha$ (Kewley et al. 2015). Therefore, the dual emitters, which tend to have the stronger [OIII] emission lines than the $H\alpha$ -single-emitters, are biased towards higher $sSFR_{UV}$.

On the other hand, a possible difference between the [OIII]-single-emitters and the dual emitters is not straightforward to interpret because the [OIII]-single-emitters should also have the stronger [OIII] emission line with respect to the $H\alpha$ emission line. At lower $sSFR_{UV}$ regime ($\lesssim -9.0$ [yr^{-1}]), the [OIII]-single-emitters show a larger fraction of galaxies as compared to the dual emitters. This may be caused by a contribution of faint AGNs, but in order to investigate the presence of AGNs in our sample, deep spectroscopy and line diagnostic analysis would be necessary. We here also note that there is a contamination of the [OIII] $\lambda 4959$ and $H\beta$ emitters in our [OIII]-single-emitters as mentioned in §2.3. These emitters would be misclassified as the [OIII]-single-emitters even if they actually have the strong $H\alpha$ emission line. In such a case, the stellar masses might be overestimated because of the contribution of $H\alpha$ (and [NII]) fluxes to the K -band fluxes. Therefore, the [OIII] $\lambda 4959$ and $H\beta$ emitters could contribute to the lower $sSFRs$ seen in the [OIII]-single-emitters.

At this point, we are not able to further investigate the cause of such difference, and we leave it for future investigation. However, it should be stressed that except for the two particular cases, the physical properties of the three emitter subsamples are not statistically different.

3.5 Biases due to the NB selection

Finally, we discuss possible biases introduced by the NB selection, which are based on the flux and EW of emission lines.

As shown in Holden et al. (2014) and Shimakawa et al. (2015), the [OIII]/ $H\beta$ ([OIII]/ $H\alpha$) ratio is correlated with $sSFR$ of star-forming galaxies in the sense that the galaxies with higher $sSFRs$ tend to show the larger [OIII]/ $H\alpha$ ratios. Given the fact that the EW of $H\alpha$ is directly proportional to $sSFR$ (e.g. Leitherer et al. 1999), the flux- and EW-limited sample might be biased towards the galaxies with the larger [OIII]/ $H\alpha$ ratios. In such a case, the $H\alpha$ and [OIII] emitters might show similar properties because the $H\alpha$ emitters tend to consist of the galaxies with the relatively strong [OIII] emission line.

Sobral et al. (2014) investigated the relation between the rest-frame EW ($H\alpha$ + [NII]) and stellar mass for the $H\alpha$ emitters at $z=0.4, 0.8, 1.5,$ and 2.2 obtained by the HiZELS project. They found that the $H\alpha$ emitters at $z \sim 1-2.2$ distribute well above the EW ($H\alpha$ + [NII]) cut of 25 \AA up to a stellar mass of $\log(M_*/M_\odot) \sim 11.5$ (Figure 3 in Sobral et al. 2014). The relation between the rest-frame EW and stellar mass was also investigated for the [OIII]+ $H\beta$ emitters by Khostovan et al. (2016). Their results show that the [OIII]+ $H\beta$ emitters at $z > 1$ have much higher EW than the EW selection limit. Therefore, it is expected, in the first place, that our samples are not strongly affected by the EW-cut. Moreover, we show that the [OIII]/ $H\alpha$ ratios of our samples are roughly consistent with those of star-forming galaxies at the same epoch in the literature as in §3.1. The [OIII]/ $H\alpha$ ratios do not seem to be largely different among the samples of star-forming galaxies selected by different methods. This indicates that our NB-selected samples are not necessarily biased towards galaxies with higher [OIII]/ $H\alpha$ ratios.

4 CONCLUSIONS

We use the NB-selected galaxy catalog at $z=2.23$ obtained by the HiZELS project, and construct the two galaxy samples of $H\alpha$ and [OIII] emission line galaxies by applying the same line flux limit. We derive the global physical properties of these emitters, and

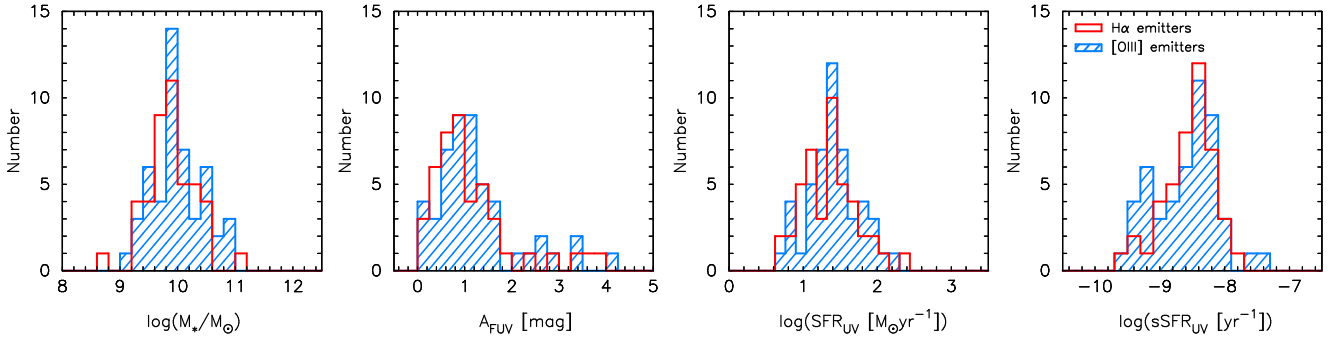


Figure 5. Number distributions of a stellar mass, dust extinction (A_{FUV}), SFR_{UV} and sSFR_{UV} from left to right. The open and hatched histograms represent H α emitters and [OIII] emitters, respectively. The p -values obtained from the KS-test are listed in Table 3.

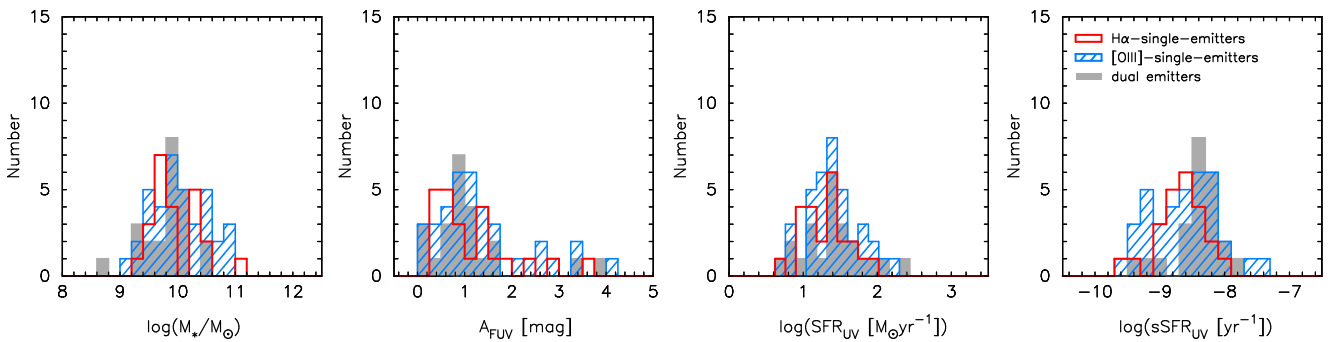


Figure 6. Number distributions of a stellar mass, dust extinction (A_{FUV}), SFR_{UV} and sSFR_{UV} from left to right. The emitter samples are divided into three subsamples, H α -single-emitters (open histograms), [OIII]-single-emitters (hatched histograms), and dual emitters (filled histograms). The p -values are listed in Table 3.

Table 3. The p -values from the KS-test of comparisons of physical quantity distributions among different emitter samples as shown in Figure 5 and Figure 6.

	M_*	A_{FUV}	SFR_{UV}	sSFR_{UV}
H α emitters versus [OIII] emitters	0.76	0.69	0.56	0.77
H α -single-emitters versus [OIII]-single-emitters	0.85	0.63	0.56	0.57
H α -single-emitters versus dual emitters	0.36	0.84	0.59	0.006
[OIII]-single-emitters versus dual emitters	0.12	0.36	0.97	0.04

compare the number distribution of a stellar mass, dust extinction (A_{FUV}), SFR_{UV} , and sSFR_{UV} between the two samples. The resulting p -values from a KS-test indicates that the H α and [OIII] emitters are drawn from the same parent population. The two galaxy populations cover almost the same ranges of the integrated properties at $z \sim 2$.

We also divide the whole sample into three subsamples, namely, the galaxies detected with either H α or [OIII] alone, and the galaxies detected with both lines. Again, a KS-test does not show any significant differences among the three subsamples, except for the dual emitters, which tend to be biased to higher sSFR_{UV} as compared to the other two subsamples. It is indicated that the strong [OIII] emission lines are likely to be related to high star formation activities (and thus high ionization parameters) of star-forming galaxies at $z \sim 2$. Note, however, the [OIII] and H α emitters used in this study could harbor low luminosity AGNs, especially the [OIII]-single-emitters with low sSFR as discussed in §3.4.2, and spectroscopic observations are necessary to confirm the presence of AGNs.

In summary, the [OIII] emitters trace almost the same galaxy

populations as the H α emitters at $z \sim 2$, and therefore we argue that the [OIII] emission line can be used as an indicator of normal star-forming galaxies at high redshifts. Our results support the importance and the effectiveness of [OIII] emitter surveys at $z \gtrsim 3$, where H α emission is no longer effectively observed from the ground.

ACKNOWLEDGEMENTS

We thank the anonymous referee for careful reading and comments that improved the clarity of this paper. TLS acknowledges to Prof. Lisa Kewley for kindly accepting the visit to Mt. Stromlo Observatory for three months. The major part of this paper was written during the stay. TLS is also grateful to her group members for the many ways in which they helped. TK acknowledges the financial support in part by a Grant-in-Aid for the Scientific Research (Nos. 21340045 and 24244015) by the Japanese Ministry of Education, Culture, Sports and Science. DS acknowledges financial support from the Netherlands Organisation for Scientific research (NWO) through a Veni fellowship,

from FCT through a FCT Investigator Starting Grant and Start-up Grant (IF/01154/2012/CP0189/CT0010) and from FCT grant PEst-OE/FIS/UI2751/2014. IRS acknowledges support from STFC (ST/L00075X/1), the ERC Advanced Grant DUSTYGAL (321334) and a Royal Society/Wolfson Merit Award. PNB is grateful for support from the UK STFC via grant ST/M001229/1.

REFERENCES

- An F. X. et al., 2014, *ApJ*, 784, 152
Atek H. et al., 2010, *ApJ*, 723, 104
Atek H. et al., 2014, *ApJ*, 789, 96
Best P. et al., 2013, *Astrophys. Space Sci. Proc.*, 37, 235
Brammer G., van Dokkum P. G., Coppi P., 2008, *ApJ*, 686, 1503
Bruzual G., Charlot S., 2003, *MNRAS*, 344, 1000
Bunker A. J., Warren S. J., Hewett P. C., Clements D. L., 1995, *MNRAS*, 273, 513
Calzetti D., Armus L., Bohlin R. C., Kinney A. L., Koornneef J., Storchi-Bergmann T., 2000, *ApJ*, 533, 682
Casali M. et al., 2007, *A&A*, 467, 777
Chabrier G., 2003, *PASP*, 115, 763
Civano F. et al., 2016, *ApJ*, 816, 62
Colbert J. W. et al., 2013, *ApJ*, 779, 34
Daddi E., Dickinson M., Morrison G., et al. 2007, *ApJ*, 670, 156
Donley J. L., Rieke G. H., Pérez-González P. G., Barro G., *ApJ*, 687, 111
Donley, J. L. et al., 2012, *ApJ*, 748, 142
Elbaz D. et al., 2007, *A&A*, 468, 33
Erb D. K., Shapley A. E., Pettini M., Steidel C. C., Reddy N. A., Adelberger K. L., 2006a, *ApJ*, 644, 813
Erb D. K., Steidel C. C., Shapley A. E., Pettini M., Reddy N. A., Adelberger K. L., 2006b, *ApJ*, 647, 128
Faisst A. L. et al. 2016, preprint, (arXiv:1601.07173)
Förster Schreiber N. M. et al., 2009, *ApJ*, 706, 1364
Garn T., Best P. N., 2010, *MNRAS*, 409, 421
Geach J. E., Smail I., Best P. N., Kurk J., Casali M., Ivison R. J., Coppin K., 2008, *MNRAS*, 388, 1473
González V., Labbé I., Bouwens R. J., Illingworth G., Franx M., Kriek M., Brammer G. B., 2010, *ApJ*, 713, 115
Hagen A. et al., 2016, *ApJ*, 817, 79
Hayashi M., Kodama T., Koyama Y., Tadaki K.-i., Tanaka I., 2011, *MNRAS*, 415, 2670
Hayashi M., Sobral D., Best P. N., Smail I., Kodama T., 2013, *MNRAS*, 430, 1042
Heinis S. et al., 2013, *MNRAS*, 429, 1113
Holden B. P. et al., 2014, preprint (arXiv:1401.5490)
Hopkins A. M., Beacom J. F., 2006, *ApJ*, 651, 142
Hopkins A. M. et al., 2003, *ApJ*, 599, 971
Ilbert O. et al., 2009, *ApJ*, 690, 1236
Kashino D. et al., 2013, *ApJ*, 777, L8
Kennicutt R. C. Jr., 1998, *ARA&A*, 36, 189
Kennicutt R. C., Evans N. J., 2012, *ARA&A*, 50, 531
Kewley L. J., Dopita M. A., Leitherer C., Davé R., Yuan T., Allen M., Groves B., Sutherland R., 2013, *ApJ*, 774, 100
Kewley L. J., Zahid H. J., Geller M. J., Dopita M. A., Hwang H. S., Fabricant D., 2015, *ApJ*, 812, L20
Kodama T., Hayashi M., Koyama Y., Tadaki K.-i., Tanaka I., Shimakawa R. 2013, in *IAU Symp. 295, The Intriguing Life of Massive Galaxies*, ed. D. Thomas, A. Pasquali, & I. Ferreras (Cambridge: Cambridge Univ. Press), 74
Khostovan A. A., Sobral D., Mobasher B., Best P. N., Smail I., Stott J. P., Hemmati S., Nayyeri S., 2015, *MNRAS*, 452, 3948
Khostovan A. A., Sobral D., Mobasher B., Smail I., Darvish B., Nayyeri H., Hemmati S., Stott J. P., 2016, preprint (arXiv:1604.02456)
Koyama Y. et al., 2013, *MNRAS*, 434, 423
Kriek M., van Dokkum P. G., Labbé I., Franx M., Illingworth G. D., Marchesini D., Quadri R. F., 2009, *ApJ*, 700, 221
Kroupa P., 2002, *Science*, 295, 82
Labbé I. et al., 2013, *ApJ*, 777, L19
Lacy M., Petric A. O., Sajina A., Canalizo G., Storrie-Lombardi L. J., Armus L., Fadda D., Marleau F. R., *AJ*, 133, 186
Leitherer C. et al., 1999, *ApJS*, 123, 3
Madau P., Pozzetti L., Dickinson M., 1998, *ApJ*, 498, 106
Malkan M. A., Teplitz H. & McLean I. S., 1996, *ApJ*, 468, L9
Marchesini D., van Dokkum P. G., Förster Schreiber N. M., Franx M., Labbé I., Wuyts S., 2009, *ApJ*, 701, 1765
Maschietto F. et al., 2008, *MNRAS*, 389, 1223
Masters D. et al., 2014, *ApJ*, 785, 15
Matthee J., Sobral D., Oteo I., Best P., Smail I., Röttgering H., Paulino-Afonso A., 2016, *MNRAS*, 458, 449
Mehta V. et al., 2015, *ApJ*, 811, 141
Meurer G. R., Heckman T. M., Calzetti D., 1999, *ApJ*, 521, 64
Miyazaki S. et al., 2002, *PASJ*, 54, 833
Moorwood A. F. M., van der Werf P. P., Cuby J. G., Oliva E., 2000, *A&A*, 362, 9
Nakajima K., Ouchi M., 2014, *MNRAS*, 442, 900
Noeske K. G. et al., 2007, *ApJ*, 660, L43
Oke J. B., Gunn J. E., 1983, *ApJ*, 266, 713
Oteo I., Sobral D., Ivison R. J., Smail I., Best P. N., Cepa J., Pérez-García A. M., 2015, *MNRAS*, 452, 2018
Pozzetti L. et al., 2007, *A&A*, 474, 443
Reddy N. A., Erb D. K., Pettini M., Steidel C. C., Shapley A. E., 2010, *ApJ*, 712, 1070
Reddy N. A., Pettini M., Steidel C. C., Shapley A. E., Erb D. K., Law D. R., 2012, *ApJ*, 754, 25
Reddy N. A. et al. 2015, *ApJ*, 806, 259
Scoville N. et al., 2007, *ApJS*, 172, 1
Salpeter E. E. 1955, *ApJ*, 121, 161
Shapley A. E. et al., 2015, *ApJ*, 801, 88
Shim H., Chary R.-R., Dickinson M., Lin L., Spinrad H., Stern D., Yan C.-H., 2011, *ApJ*, 738, 69
Shimakawa R., Kodama T., Tadaki K.-i., Hayashi M., Koyama Y., Tanaka I., 2015, *MNRAS*, 448, 666
Shimakawa R. et al., 2016, *MNRAS*, submitted
Silverman J. D. et al., 2015, *ApJS*, 220, 12
Smit R. et al., 2014, *ApJ*, 784, 58
Smit R., Bouwens R. J., Labbé I., Franx M., Wilkins S. M., Oesch P. A., 2015, preprint (arXiv:1511.08808)
Sobral D. et al., 2009, *MNRAS*, 398, 75
Sobral D., Best P. N., Matsuda Y., Smail I., Geach J. E., Cirasuolo M., 2012, *MNRAS*, 420, 1926
Sobral D., Smail I., Best P. N., Geach J. E., Matsuda Y., Stott J. P., Cirasuolo M., Kurk J., 2013, *MNRAS*, 428, 1128
Sobral D., Best P. N., Smail I., Mobasher B., Stott, J., Nisbet D., 2014, *MNRAS*, 437, 3516
Sobral D. et al., 2015, *MNRAS*, 451, 2303
Sobral D., Kohn S. A., Best P. N., Smail I., Harrison C. M., Stott J., Calhau J., Matthee J., 2016, *MNRAS*, 457, 1739
Stark D. P., Ellis R. S., Bunker A., Bundy K., Targett T., Benson A., Lacy M., 2009, *ApJ*, 697, 1493
Stark D. P., Schenker M. A., Ellis R. S., Robertson B., McLure R., Dunlop J., 2013, *ApJ*, 763, 129
Steidel C. C. et al., 2014, *ApJ*, 795, 165
Stern D. et al., 2005, *ApJ*, 631, 163
Storey P. J., Zeppen C. J., 2000, *MNRAS*, 312, 813
Stott J. P. et al., 2014, *MNRAS*, 443, 2695
Stroe A., Sobral D., 2015, *MNRAS*, 453, 242
Suzuki T. L. et al., 2015, *ApJ*, 806, 208
Tadaki K.-i., Kodama T., Tanaka I., Hayashi M., Koyama Y., Shimakawa R., 2013, *ApJ*, 778, 114
Tasca L. A. M. et al., 2015, *A&A*, 581, 54
Teplitz H. I., Malkan M. A., McLean I. S., 1999, *ApJ*, 514, 33
Tremonti C. A. et al., 2004, *ApJ*, 613, 898
Troncoso P. et al., 2014, *A&A*, 563, 58
Whitaker K. E. et al. 2011, *ApJ*, 735, 86

Whitaker K. E. et al. 2014, ApJ, 795, 104

Williams R. J., Quadri R. F., Franx M., van Dokkum P., Labbé I., 2009, ApJ, 691, 1879

Wuyts S. et al., 2007, ApJ, 655, 51

Zakamska N. L., Strauss M. A., Heckman, T. M., Ivezić Z., Krolik J. H., AJ, 2004, 128, 1002

This paper has been typeset from a \TeX/L\AA\TeX file prepared by the author.